

RSC Advances



This is an *Accepted Manuscript*, which has been through the Royal Society of Chemistry peer review process and has been accepted for publication.

Accepted Manuscripts are published online shortly after acceptance, before technical editing, formatting and proof reading. Using this free service, authors can make their results available to the community, in citable form, before we publish the edited article. This *Accepted Manuscript* will be replaced by the edited, formatted and paginated article as soon as this is available.

You can find more information about *Accepted Manuscripts* in the [Information for Authors](#).

Please note that technical editing may introduce minor changes to the text and/or graphics, which may alter content. The journal's standard [Terms & Conditions](#) and the [Ethical guidelines](#) still apply. In no event shall the Royal Society of Chemistry be held responsible for any errors or omissions in this *Accepted Manuscript* or any consequences arising from the use of any information it contains.



Spectroscopic markers for uranium(VI) phosphates: a vibronic study

E. Faulques,^{a†} N. Kalashnyk,^{b†} F. Massuyeau,^{a†} and D. L. Perry^{c†}

Received 00th January 20xx,
Accepted 00th January 20xx

DOI: 10.1039/x0xx00000x

www.rsc.org/

Optical spectroscopic fingerprints of several uranium phosphates relevant for environmental sustainability have been determined. The studied minerals contain uranium(VI) cation coordination centers linked to phosphate functional groups and water molecules. Easy and fast identification of these minerals in their bulk state is possible by using either Raman, infrared, optical, or photoluminescence spectroscopy. Simple density functional theory vibrational modeling is presented to identify the main vibrational lines. These affordable methods of spectroscopy can be readily employed in optical remote sensing to identify uranyl species in groundwater, soil, or other geologic samples and in biological specimen for the purpose of tracking radionuclide transport, pollution, and of soluble uranium remediation by uranyl phosphates precipitation.

1 Introduction

Natural minerals in the environment can afford a wonderful registry for studying structure and bonding of uranium. On a geologic timescale, uranium has incorporated itself into over two hundred minerals that are found naturally occurring in the Earth's crust. These minerals become very pertinent in a wide variety of scientific and technological endeavors that include mining,^[1,2] metallurgy,^[3,4] nuclear energy for fuel,^[5,6] medicine,^[7,8] environmental research,^[9,10] and oceanography.^[11,12] As a matter of fact, hexavalent uranium(VI) is present in all of these mineral varieties and is able to migrate with different retention rates through the environment. It is therefore crucial to understand the properties of uranium(VI) cations within minerals and their interactions with soils, groundwater, coals, or fertilizers. These investigations require a full characterization with modern spectroscopic tools probing the uranyl cation (UO_2^{2+}) in different chemical environments. Uranyl phosphate minerals provide an excellent experimental system for this goal, because they include uranium ions interacting with the natural environment leading to the formation of real-life solid state uranium phases. By iterative investigations of the uranium phosphate minerals, more and more details will emerge on their bonding, both intrinsic and relative to one another.

On the other hand, U^{VI} is a major contaminant in many groundwater settings where it is highly mobile and soluble. Therefore, environmental transport of this heavy metal species is

potentially hazardous for environment, agriculture, and populations since it can cause cancer due to its radioactivity and chemistry. Chemical toxicity effects are notorious in the case of depleted uranium dust being absorbed in vitro. To overcome these environmental and health issues, remediation of soluble U^{VI} can be achieved by direct precipitation of uranyl phosphate minerals using polyphosphate.^[13]

In this work we use a combination of several optical spectroscopic techniques on uranyl phosphate hydrates minerals to provide vibrational models and vibrational/electronic signatures permitting to track these compounds in the environment. The minerals studied are metatorbernite $[\text{Cu}(\text{UO}_2\text{PO}_4)_2 \cdot 8(\text{H}_2\text{O})]$,^[14] phosphuranlyite $[\text{KCa}(\text{H}_3\text{O})_3(\text{UO}_2)_2(\text{PO}_4)_4 \cdot 8\text{H}_2\text{O}]$,^[15] saleeite $[\text{Mg}(\text{UO}_2\text{PO}_4)_2 \cdot 10\text{H}_2\text{O}]$,^[16] ulrichite $[\text{CaCu}(\text{UO}_2)(\text{PO}_4)_2 \cdot 4\text{H}_2\text{O}]$,^[17] and uranocircite $[\text{Ba}(\text{UO}_2)_2(\text{PO}_4)_2 \cdot 10\text{H}_2\text{O}]$,^[18] all of which contain a structural coordination core of hexavalent uranium surrounded by both the oxygen atoms combined with uranium to form uranyl cations and the oxygen atoms donated by the anionic phosphate functional group and water molecules. The present results constitute a comprehensive study comparing at once these uranyl phosphate minerals by means of four complementary optical spectroscopy tools with the support of empirical and density functional theory (DFT) calculations. We show that the discrimination of different uranyl phosphate species is possible by using vibrational and electronic spectroscopy, typically Raman, infrared, optical reflectance and photoluminescence techniques. They yield fingerprints specific for each of the minerals which can be afterwards easily tracked in groundwater, soil, or other geologic samples. In the solid state, vibrational frequencies of the uranyl ion and room-temperature energies of the absorption and emission vary from one sample to another due to their sensitivity to the uranium coordination sphere. Multiple optical techniques combined to calculations performed here represent an original approach to identifying unambiguously specific spectral signatures of uranyl phosphate hydrates. To our knowledge, UV-visible diffuse reflectance spectra for the five minerals and first-principles estimates of their vibrations are also reported for the first time.

^a Institut des Matériaux Jean Rouxel, Université de Nantes, UMR CNRS 6502, 2 rue de la Houssinière, BP 32229, F-44322 Nantes, France. Email : eric.faulques@cncrs-imn.fr

^b Institut Matériaux Microélectronique Nanosciences de Provence, Université d' Aix-Marseille, UMR CNRS 7334, F-13397 Marseille Cedex 20, France

^c Lawrence Berkeley National Laboratory, University of California, Mail Stop 70A1150, Berkeley, CA 94720, USA

† These authors contributed equally.

Electronic Supplementary Information (ESI) available: extraction of spectral information, DFT calculation methodology, modified spectral presentations and additional tables of frequencies and vibronic gaps. See DOI: 10.1039/x0xx00000x

Consequently, direct speciation of uranium in the as-formed minerals by photon-induced spectroscopic techniques can be operative without subsequent sample dissolution, and has a strong potential i) to substitute conventional time-demanding chemical analyses employed in mineralogy and ii) to be applied for remote sensing of the environment.

2 Experimental

2.1 Minerals samples

The certified minerals were obtained from Mineralogical Research Company (Minresco), San Jose, CA, USA, and used as received. Geographical origins of the studied minerals are given in Table 1.

Table 1 Origin of the minerals investigated in this study

Mineral	Geographical origin
Ulrichite	Lake Boga Granite, Quarry, Northwest Victoria, Australia
Uranocircite	Bergen, near Falkenstein, Vogtland, Saxony, Germany
Metatorbernite	3miles SO. of Crown King, Bradshaw Mts., Yavapai Co., Arizona, USA
Saleeite	East Alligator River, Northern Territory, Australia
Phosphuranylite	Bedford, Westchester County, New York, USA

Metatorbernite and saleeite were provided as green crystalline flakes of dimensions up to $3 \times 3 \times 0.2$ mm³. Phosphuranylite and uranocircite powdery samples were gently scratched from the rocky stones on which they were lying and were studied as yellow tiny crystals. Finally, ulrichite is the rarest sample among all, and we had about 1 mm³ of green, tiny acicular crystals radiating from the matrix of a rock fragment. This mineral is only found in a unique location in Australia (see Table 1).

2.2 Spectroscopic techniques

Raman analyses were carried out employing two confocal Raman microprobes (Horiba Jobin-Yvon T64000 and Renishaw inVia microscope) coupled with an optical microscope and equipped with Kr⁺ and diode laser sources (λ_0 equal to 647.1 nm and 785 nm), and diffraction gratings of 1800 and 1200 grooves per mm. Spectra were collected in the ranges between 100 and 2000/4000 cm⁻¹. Crystals were placed and orientated on the stage of the microscopes equipped with 10 \times , 20 \times , 50 \times and 100 \times objectives. The diameter of the laser spot on the sample surface was ~ 2 to 4 μ m for the fully focused laser beam at 100 \times and 50 \times objective magnifications, respectively. Photoluminescence experiments were carried out using i) a confocal Raman microprobe (Horiba Jobin-Yvon LabRam) coupled with an optical microscope with a 40 \times objective magnification and equipped with a UV CdHe laser source ($\lambda_0 = 325$ nm), the results are presented here; ii) a fluorimeter Horiba Jobin-Yvon Fluorolog with several excitations, the results are presented in Supplementary Information. All Raman instruments were calibrated against the Stokes Raman signal of pure Si at 520

cm⁻¹ using a silicon wafer. The spectral resolution was ~ 2 cm⁻¹. Fourier-transform Infrared (FTIR) absorption spectra were obtained on a Bruker Vertex instrument using an attenuated total reflectance (ATR) apparatus (Goldengate, Specac) between 400 and 4000 cm⁻¹ with a resolution of 4 cm⁻¹. UV-visible absorption experiments were performed using a Perkin Elmer UV-visible-IR spectrometer (Lambda 1050) with an integrating sphere designed to measure the diffuse reflectance of solid samples. The very small quantity of ulrichite compelled us to carry out only a limited number of spectroscopic investigations. For this reason, single ATR and UV-visible reflectance experiments could not be repeated and involved a very small amount of ulrichite crystals (less than 500 μ m²) not covering fully the sample holder or the ATR diamond crystal. This was not a limitation for micro-Raman spectroscopy, since this technique is able to probe samples up to 1 μ m size and constitutes a major advantage in the identification of the minerals.

Spectral bands have been decomposed into their vibrational components by fitting them to several functions to determine more precisely their position.

2.3 DFT methodology

Vibrational frequencies of phosphate and uranyl ions were calculated using density functional theory with the Gaussian09 and Q-Chem suite of programs (see Supplementary Information). The uranium and phosphorus atoms were described by effective core pseudo-potentials (ECP) and their associated basis sets. Since uranium is a heavy atom, we have taken a relativistic basis set (Stuttgart RLC ECP) as already evaluated in uranyl complexes with exchange-correlation hybrid functional (XC) B3LYP.^[19,20] For the P atom we use the LANL2DZ basis set and the PBE XC functional. The O atom in the ions was described using the 6-311++G** basis set including one set of polarizations and one set of diffuse functions. Calculations were performed at Centre de Calcul Intensif des Pays de la Loire (CC IPL), Nantes.

3 Results and discussion

The five uranium phosphate minerals studied here have been the focus of previous, rigorous structural studies by single-crystal X-ray diffraction crystallography (XRD).^[14-18] Accordingly, vibrational data such as Raman scattering can be combined with theoretical and modeling efforts based on known exact bond angles and distances. Furthermore, this work benefits from a comparison basis with Raman and infrared (IR) spectra of several uranyl phosphate minerals compiled in the RRUFF™ database^[21] as well as in papers of Cejka et al.,^[22] Frost et al.,^[23-26] and in the recent comprehensive study of Driscoll et al.^[27] of 13 different uranyl minerals. Synthetic uranyl compounds including metatorbernite and metauranocircite have also been studied with vibrational spectroscopy in several previous works.^[28-32]

3.1 DFT calculation of uranyl and phosphate frequencies.

In this work, empirical and DFT frequency calculations were performed to confirm the current experimental results and to provide the most probable vibrational assignments. The uranyl ion present in the investigated minerals is often slightly bent with approximate point group symmetry C_{2v} (here for simplification we consider that U–O bond lengths are equal, which is not always the case in real crystals). The representation of vibrations is $\Gamma_{\text{vib}} = 2A_1 + B_1$, therefore they are all active in IR and Raman. The A_1 denotes the O–U–O symmetric stretching and the bending O–U–O modes with

frequency ν_1 and ν_2 , respectively, and B_1 the asymmetric O–U–O stretching mode with frequency ν_3 . The isolated phosphate ion is tetrahedral with point group symmetry T_d yielding vibrations represented by $\Gamma_{\text{vib}} = A_1 + E + 2T_2$. All these harmonic nuclear motions are Raman active, while only the triply degenerate T_2 modes are IR active in the gas state. Frequencies of symmetric and antisymmetric P–O stretching modes A_1 and T_2 are labeled ν_1 and ν_3 , respectively; and symmetric and antisymmetric P–O bending modes E (doubly degenerate) and T_2 are labeled ν_2 and ν_4 , respectively.

The U–O bond lengths and stretching frequencies of uranyl ions can be determined from X-ray data using the empirical Badger's rule (BR)^[33,34] or the more recent Bartlett and Cooney (BC)^[35] relationships:

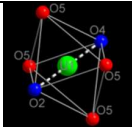
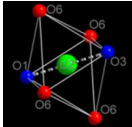
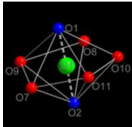
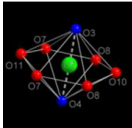
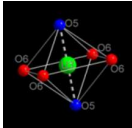
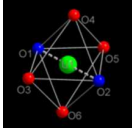
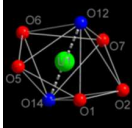
$$d_{\text{U-O}} = 1.08k^{-1/3} + 1.17 \text{ \AA} \text{ (BR)} \quad (1)$$

$$d_{\text{U-O}} = 106.5\nu_1^{-2/3} + 0.575 \text{ \AA} \text{ (BC1)}$$

$$d_{\text{U-O}} = 91.42\nu_3^{-2/3} + 0.804 \text{ \AA} \text{ (BC2)}$$

where $d_{\text{U-O}}$ is the length, and k the force constant of the U–O bond which enable comparison with the observed values. The empirically computed values of frequencies using the above equations are given in Tables 2 and S1 together with those calculated with DFT.

Table 2 Experimental and unscaled calculated frequencies of the uranyl cations in the minerals^{a-c}

Materials	Observed Uranyl Sites	Distances (Å) and Angles (°)	Observed Frequencies (cm ⁻¹)			Calculated Frequencies (cm ⁻¹)		
			ν_2	ν_1	ν_3 (Raman/IR)	ν_2	ν_1	ν_3
Metatorbernite		U ₁ -O ₂ :1.770	303	826	905/906	291	734	879
		U ₁ -O ₄ :1.816					841	935
		O ₂ -U ₁ -O ₄ :180					795	873
		U ₂ -O ₁ :1.775	285			283	790	893
		U ₂ -O ₃ :1.780					836	929
		O ₁ -U ₂ -O ₃ :180					831	921
Phosphuranylite		U ₁ -O ₁ :1.811	239	813	NA /876-902	239	719	836
		U ₁ -O ₂ :1.795					800	879
		O ₁ -U ₁ -O ₂ :178.5					815	900
		U ₂ -O ₃ :1.771	264	827		283	770	887
		U ₂ -O ₄ :1.797					840	934
		O ₃ -U ₂ -O ₄ :178.2					814	898
		U ₃ -O ₅ :1.778	283	840		284	788	891
		O ₅ -U ₃ -O ₅ :180					833	924
Saleeite		U ₁ -O ₁ :1.744	284	837	NA/901	269	840	954
		U ₁ -O ₂ :1.768					870	975
		O ₁ -U ₁ -O ₂ :179.6					843	939
Ulrichite		U ₁ -O ₁₂ :1.807	291	812	NA/880	298	673	802
		U ₁ -O ₁₄ :1.841					804	884
		O ₁₂ -U ₁ -O ₁₄ :177.5					772	841

PAPER							RSC Advances	
Metauranocircite II		U ₁ -O ₁ :1.808	289	823	905/877-905	277	758	931
		U ₁ -O ₂ :1.746					803	883
		O ₁ -U ₁ -O ₂ :175.2					867	972
		U ₂ -O ₃ :1.748	289			277	773	931
		U ₂ -O ₄ :1.801					865	969
		O ₃ -U ₂ -O ₄ :176.5					810	892

^aThe distances and angles are taken from the observed XRD structures. ^bUranocircite observed frequencies have been modeled by taking the metauranocircite II structure containing 6H₂O. ^cDFT frequencies (upper rows); basis sets for O: 6-311++G** and U: Stuttgart RLC ECP with B3LYP exchange-correlation functional. Empirical calculations based on Eq. 1 for pairs of U–O bonds are given in italics below DFT values. Only observed frequencies *in correspondence* with calculated ones are reported. Ions are isolated from the crystals without environment effects.

The empirical relationships above presume that either the distances, force constants or the frequencies of the ions are known. These estimates were advantageously completed by DFT predictions of vibrational frequencies of the molecular moieties in these minerals. These calculations support well the empirical assignment of uranyl and phosphate vibrations (Tables 2 and 3). All frequencies seem to be remarkably reproduced even if ν_1 and ν_3 of uranyl in phosphuranylite and ulrichite present discrepancy with observed lines. The calculated frequencies of the isolated phosphate ion match also well the experiments if we compare them with DFT vibrational calculations of PO₄³⁻ already published^[36] and taking into account that our assignment is partly based on previous

references.^[25-28] The symmetric ν_2 and antisymmetric ν_4 phosphate vibrations tentatively ascribed here to experimental vibrational lines from DFT prediction are found to be moderately lower than the assignment previously proposed in the literature.^[28] In this work, under- or overestimated values have not been scaled in order to reproduce the observed values. One can note also that the present DFT calculation does not take into account the static crystal field and environment effects on the vibrational frequencies of the as-calculated ions, nor spin-orbit coupling. In the real cases, dispersive forces, spatial overlap of the electronic densities, dynamical Coulomb coupling, electron-phonon interaction can influence internal frequencies.

Table 3 Experimental and corresponding unscaled calculated DFT frequencies of the phosphate anion in the minerals^{a-c}

Materials	Distances (Å) and Angles (°)	Observed Frequencies (cm ⁻¹)				Calculated Frequencies (cm ⁻¹)			
		ν_2	ν_4	ν_1	ν_3	ν_2	ν_4	ν_1	ν_3
Metatorbernite	P-O _{1,4} :1.53 110.2	124	288	(790)	980	148	267	788	977
		223	401		1105	242	406		1120
			440		1128		417		1133
Phosphuranylite	P-O ₁ :1.504 103.5	237	398	981	1034	228	401	942	1035
	P-O ₂ :1.526 108.6	282	-	1004	1086	282	405		1098
	P-O ₃ :1.556 109.0		441		1195		430		1212
	P-O ₄ :1.571 109.7								
Saleeite	P-O ₁ :1.50 106.3	194	405	987	1025	230	396	924	1010
	P-O ₂ :1.53 109.4	286		999	1112	285	417		1114
	P-O ₃ :1.56 111.8						423		1200
	P-O ₄ :1.58 113.5								
Ulrichite	P-O ₁ :1.53 111.5			975	1077	198	395	974	1087
	P-O ₂ :1.53 102.8			1009		313	401		1109

	P-O ₃ :1.54	112.2		458	1028		446		1160
	P-O ₄ :1.54	113.1							
Metauranocircite II	P-O ₁ :1.47	105.9	200		989	1095	204	378	1024
	P-O ₂ :1.49	108.5	291	401		1116	269	395	
	P-O ₃ :1.50	109.7				1160		418	1316
	P-O ₄ :1.54	110.9							

^aThe distances and angles are taken from a *single site* of the observed XRD structures. ^bUranocircite observed frequencies have been modelled by taking the metauranocircite II structure containing 6H₂O. ^cBasis set LANL2DZ, with Perdew-Burke-Ernzerhof (PBE) exchange-correlation functional. Ions are isolated from the crystals without environment effects.

3.2 Micro-Raman spectra of the uranyl minerals.

Micro-Raman spectra of the minerals are presented in Fig. 1. Using red excitation sources at 785 nm and 647 nm mitigates fluorescence of the uranyl cation in the samples which could mask the Raman signal. Several groups of parent lines can be distinguished for all minerals. These lines undergo more or less pronounced shifts from one mineral to another, allowing for their identification.

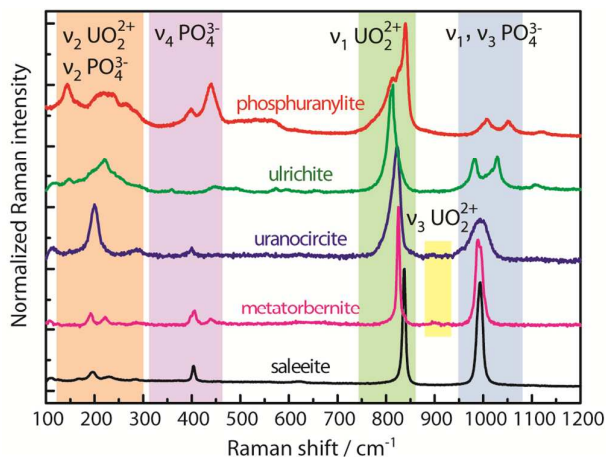


Fig. 1 Raman spectra of the five minerals taken for excitations $\lambda_0 = 647.1$ nm (1.91 eV) in phosphuranylite and 785 nm (1.58 eV) in others.

The most intense lines appear in the region of 800 cm⁻¹. This band is related to the vibrational frequencies of the UO₂²⁺ cation ascribed to the symmetric (ν_1) stretching. When examining in detail the ν_1 band close to 800 cm⁻¹ one notices that it presents a broad structure with subcomponents for phosphuranylite, ulrichite and uranocircite. For instance phosphuranylite reveals up to four subpeaks in this intense Raman band, as noticed also by Frost et al. and Driscoll et al.^[26,27] The reason for this complexity lies in the crystallographic structure of the minerals. It must be noted (see Table 1) that in all of them, the U–O bond lengths deduced from X-ray crystallography are not equivalent in several uranyl sites, giving different observed values. Furthermore, ions in the crystal occupy sites with symmetry lower than in the free state yielding to the splitting of degenerate modes and activation of modes otherwise inactive in the IR or Raman spectra. Therefore, the Raman spectra show multiple ν_1 bands ascribed to each of the U–O bond

symmetric stretching mode or corresponding to each uranyl site. On the other hand, the O–U–O antisymmetric stretching bands ν_3 are discernable with very weak intensity around 905 cm⁻¹ only for metatorbernite and uranocircite, while they are strongly activated in the IR (see below).

Thus, from the Raman experiment, the relative position of the most intense lines varies considerably with the coordination sphere of the uranyl cation. The observed and calculated frequencies with the U–O bond lengths are reported in Table 2. The DFT calculations predict that the uranyl bending vibrations (ν_2) can be expected to lie below 300 cm⁻¹, and several Raman bands are indeed found in this range. Taking into account a calculated bending force constant value k' comprised between 0.328 m dyn Å rad⁻² (198 kJ mol⁻¹ rad⁻²) and $\sim k/10$ for the uranyl cation^[37] one can anticipate that the bending frequency could appear between 147 and 220 cm⁻¹. We ascribe some experimental Raman lines occurring between 150 cm⁻¹ and 300 cm⁻¹ to the bending mode frequency ν_2 of uranyl (Fig. 1) without excluding the possibility of ν_2 additional bands appearing up to 350 cm⁻¹ due to site symmetry relaxation.

The range 120–460 cm⁻¹ in all Raman spectra could be also ascribed to the phosphate PO₄³⁻ ligand as suggested by the DFT calculations (Table 3). Some of these lines correspond to the symmetric bending and deformation (or antisymmetric bending) vibrations of the doubly (ν_2) and triply degenerate (ν_4) modes. The group of lines appearing in the 950–1150 cm⁻¹ range stems from the symmetric (ν_1) and antisymmetric (ν_3) stretchings of the PO₄³⁻ anion. In fact, the experimental region between 950 and 1100 cm⁻¹ contains overlapping lines which complicate the assignment of uranyl or phosphates ion vibrations. This assignment has been controversial in other vibrational studies of uranyl phosphates. Our calculations indicate that the antisymmetric uranyl stretching-mode frequency ν_3 should appear below 950 cm⁻¹. Therefore, the intensive lines around 1000 cm⁻¹ (green band in Fig. 2b) can be ascribed only to stretching vibrations of phosphate groups. These wavenumber (wn) ranges agree well with our DFT calculations.

Our spectrum of natural metatorbernite is identical to that found by Sanchez-Pastor et al.^[28] on synthetic metatorbernite, with major lines appearing almost at the same positions. In this mineral the O–U–O stretchings occur at 826 cm⁻¹ (ν_1) and 900–905 cm⁻¹ (ν_3). Several O–U–O bending vibrations are observed with ν_2 ranging from 196 to 283 cm⁻¹.

To summarize for this part, Raman scattering is a strong probe providing markers of each mineral in the solid-state, and it is preferable to use the most intense lines grouped around 800 cm⁻¹ (UO₂²⁺ ν_1 band region) as tracers for mineral speciation.

3.3 Attenuated total reflectance

Using FTIR-ATR technique and with help of calculations, three main groups of vibrational bands can be distinguished in the infrared spectra of the uranyl phosphates (Fig. 2a, and Tables 2, 3, 4): the regions 400–550 cm^{-1} (bending modes ν_4 of PO_4^{3-}), 850–1150 cm^{-1} (stretching modes ν_3 of UO_2^{2+} and PO_4^{3-}), ~1570–1720 cm^{-1} and ~2800–3700 cm^{-1} (water and hydroxyl broad bands, respectively). The ATR measurement insures that no atmospheric water or moisture contaminates the spectra, and that genuine water-bonded (as a true water ligand) species are probed within the material.

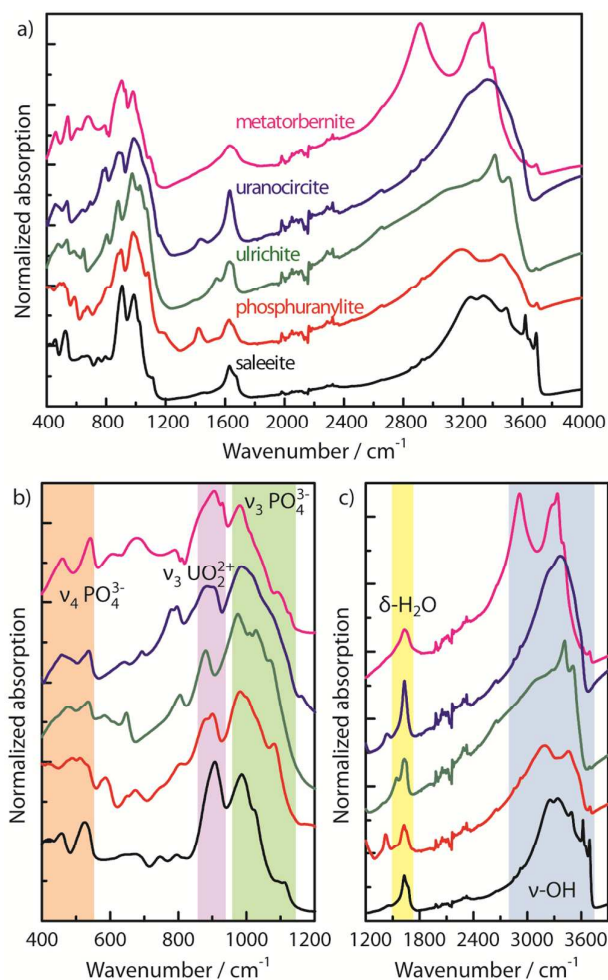


Fig. 2 FTIR ATR spectra of the five uranyl phosphate minerals on three different wn scales.

All minerals show strong OH absorptions dominating over the other bands (Figs. 2a and 2c, Table 4). In addition to the uranyl and phosphates frequencies in IR absorption, the frequencies of water signals give also excellent tracers to distinguish the minerals, as seen for example by the very singular $\nu\text{-OH}$ stretching absorption of metatorbernite (Fig. 2c) split and shifted to lower wn.

The vibrations of water in metatorbernite and saleeite correspond well to those described in the RRUFF™ database,^[21] by Cejka et al.,^[22] and Frost.^[23] The bands at ~1630 cm^{-1} correspond to the δ_{OH} bending of H–O–H groups. The positions of the δ_{OH} bands in saleeite (line at 1630 cm^{-1} and strong shoulder at 1673 cm^{-1}) and in metatorbernite (broad line with a maximum at 1631 cm^{-1}) agree

with the features reported earlier.^[23] However, it is difficult to establish a correlation between the absorption strength of the OH bands and the quantity of water bound to the structure with respect to the compounds formulae.

Table 4. H–O–H bending and $\nu\text{-OH}$ stretching infrared frequencies observed for the uranyl phosphate hydrates minerals. s: strong intensity, sh: shoulder, w: weak intensity. In italics: superimposed to the broad water absorption but not stemming from water.

Mineral	frequencies (cm^{-1})
Ulrichite	1508sh, 1544s, 1615sh, 1630s, 1649 s, 2656w, 2930sh, 3096sh, 3273w, 3364sh, 3413 s, 3505 s, 3694w
Uranocircite	1542sh, 1593sh, 1619sh, 1631 s, 1648sh, 2652w, 2853w, 2925w, 3065sh, 3238s, 3368s, 3520sh, 3589sh
Metatorbernite	1543sh, 1631s, 1669sh, 2656sh, 2914s, 3272s, 3333s, 3400sh, 3621w, 3694w
Saleeite	1552sh, 1612sh, 1630s, 1673s, 2658w, 2855w, 2928w, 3097sh, 3251s, 3340s, 3490s, 3620s, 3646sh, 3691s
Phosphuranylite	1520sh, 1543sh, 1600sh, 1627s, 1650sh, 1730wsh, 2656w, 2853w, 2929sh, 3060sh, 3193s, 3462s, 3559sh, 3596w

As suggested by Frost^[23] the number of H–O–H and $\nu\text{-OH}$ lines in the regions 1550–1700 cm^{-1} and 3200–3600 cm^{-1} should be related to water molecules involved in different H-bonds. Minerals showing the most complex H–O–H band are ulrichite, saleeite, and phosphuranylite. In general, if the frequency of the H–O–H bending mode is greater than 1630 cm^{-1} , one can expect, like in saleeite (a strong line appears superimposed at 1673 cm^{-1}), the presence of coordinated and chemically bonded water. In this mineral, the complex broad structure of the $\nu\text{-OH}$ band between 3000 and 3700 cm^{-1} confirms this observation. The same remark can be drawn for phosphuranylite, ulrichite, and metatorbernite showing a broadening of the line at ~1630 cm^{-1} due to the presence of a strong shoulder line at 1649, 1650, 1669 cm^{-1} respectively. However, in ulrichite a relatively intense line emerges also at a lower wn (1544 cm^{-1}) with a frequency near that of vapor which indicates the presence of free water molecules.

The group of sharp narrow lines between 3590 and 3700 cm^{-1} (here 2 or 3 lines) appearing for all minerals, and very intense for saleeite, could be ascribed to $\nu\text{-OH}$ groups linked to metals (M–OH)^[38] or to free H_2O molecules, with very small H-bonding interaction among $\nu\text{-OH}$ groups. The strong intensity of these lines in saleeite is likely correlated to the high number of moles of water in the structure. In metatorbernite the intensive downshifted peak at 2914 cm^{-1} reveals hydrogen bonded $\nu\text{-OH}$ groups. The IR bands at 3505 cm^{-1} in ulrichite, 3520–3589 cm^{-1} in uranocircite, and 3559–3596 cm^{-1} in phosphuranylite can be attributed to OH⁻ groups.^[39]

The intensive IR bands appearing at 880 cm^{-1} (ulrichite), 887, 905 cm^{-1} (uranocircite), ~880–904 cm^{-1} (phosphuranylite), 906 cm^{-1} (metatorbernite), and 908 cm^{-1} (saleeite) are assigned to the antisymmetric stretching modes ν_3 of UO_2^{2+} (Fig. 2b).^[22] The

positions of the experimentally observed IR ν_3 bands agree well with the calculated values (Table 2). Like in the Raman counterpart, the uranyl IR absorption of phosphuranylite reveals at least three peaks around 900 cm^{-1} corresponding to three uranyl site frequencies. Metatorbernite and uranocircite present an uranyl absorption with at least two subbands corresponding to the two uranyl sites of the structures. The antisymmetric bendings ν_4 of phosphate ions give IR bands located experimentally at 458 cm^{-1} and likely at $526\text{--}540\text{ cm}^{-1}$ while the vibrations calculated by DFT are not higher than 446 cm^{-1} . The antisymmetric ν_3 stretchings of phosphate ions are calculated in the range 977 cm^{-1} to 1318 cm^{-1} , and therefore the massif of peaks in this frequency range is correctly assigned in the IR experiment (Table 3).

3.4 Photoluminescence and diffuse reflectance spectra

The uranyl(VI) cation in minerals is well known for its strong phosphorescence in the green range of the visible spectrum.^[40-43] In the presence of phosphates groups in a metal ion environment, uranyl cations strongly phosphoresce with characteristic emission energies grouped in a typical «uranyl comb» or fine structure (Fig. 3a). The origin of this comb-like emission is vibronic by nature, with emission energies separated by intervals corresponding to the energy ν_1 of the U–O bond stretching. The energy gaps measured are around 814 , 794 , 826 , 835 cm^{-1} ($\pm 10\text{ cm}^{-1}$) for uranocircite, ulrichite, metatorbernite, and saleeite, respectively (see Table S2 in Supplementary Information). Within the estimated accuracy, the values match well the ν_1 O–U–O Raman stretching frequency, except for phosphuranylite since its PL spectrum is almost non-structured at room temperature. The relative positions of the fine structures vary with the nature of the mineral (see dotted lines in the wavelength λ scale).

Strikingly, we notice the appearance of small shoulder peaks at the highest energy side which are the so-called “hot bands” indicated by arrows in Fig. 3a. These features can be clearly seen in metatorbernite, saleeite, and ulrichite. The gap between the first high energy peak and the hot band corresponds to the O–U–O symmetric stretching frequency of the excited uranyl state. The gap values found from PL spectral fits for the three minerals above are respectively 712 , 700 , and 686 cm^{-1} (see Table S2).

Complementary electronic information to photoluminescence data has been gained by collecting UV-vis diffuse reflectance spectra of these minerals for the first time to our knowledge. Three of the minerals (saleeite, metatorbernite, uranocircite) show a striking sequence of intensive uranyl electronic transitions between 400 and 550 nm (see Fig. 3b) that are shifted towards higher energy compared to the PL spectra. Absorption profile maxima are at 428 nm (metatorbernite), 426 nm (uranocircite), 423 nm (saleeite), 435 nm (phosphuranylite), and 422 nm (ulrichite). These rich-featured spectra exhibit up to ten or more electronic transitions forming a very clear vibronic structure which mirrors that of the PL spectra. The average separation in the fine structures of reflectance is also $\sim 700\text{ cm}^{-1}$ (Table S2) confirming well the hot band gaps found in PL spectra. These excited energy gap values are significantly lower than the ν_1 stretching frequencies observed both in the Raman and PL spectra. This observation means that the electronic excited state has a U–O bond stretching force constant k^* lower than that in the ground state, and, accordingly, the d_{UO}^* distance in the excited state is larger.^[44] Taking an excited vibrational stretching frequency $\nu_1^* = 700\text{ cm}^{-1}$, one can estimate that $k^* = 4.618\text{ mdyne}\text{\AA}^{-1}$ which gives $d_{\text{UO}}^* = 1.818\text{ \AA}$, a bond distance larger than the average distances given in Table 2.

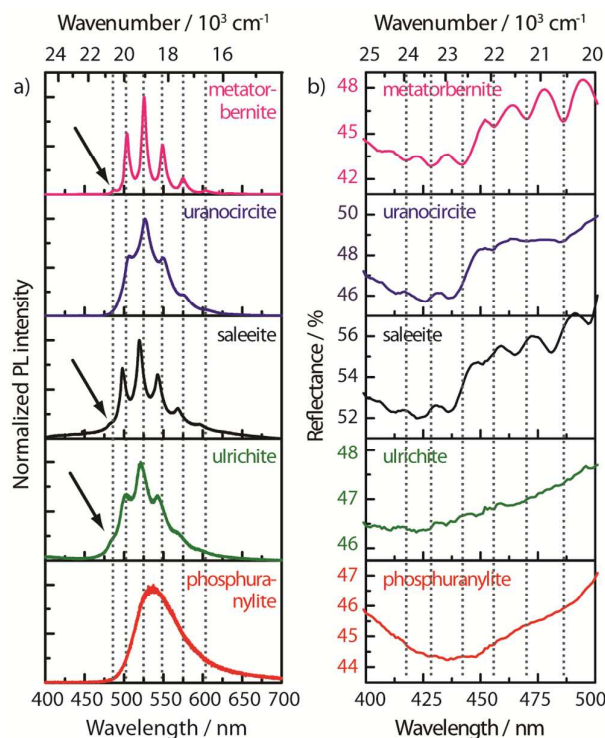


Fig. 3 (a) Photoluminescence spectra of the five uranyl phosphate minerals for excitation $\lambda_0 = 3.81\text{ eV}$ (325 nm) with Raman microprobe (see Fig. S1 for data acquired with a fluorimeter and Fig. S2 for linear wavenumber scale with λ^2 corrected intensities). The dotted lines are guides to the eyes showing peak shifts from one crystal to another. (b) Mineral-dependent UV-visible diffuse reflectance spectra with vibronic structures. See Fig. S3 for reflectance spectra between 1.908 and 4.133 eV ($300\text{--}650\text{ nm}$).

Another interesting point is the lack of sharp vibronic features in the UV-vis spectrum of phosphuranylite following the trend observed in the featureless PL spectrum. The reflectance spectrum of ulrichite is also very noisy and presents at first sight a flat, monotonic profile without discernable features. However, when analyzing the reflectance signal on a closer scale, one can distinguish several resolved transitions of very weak intensity (Fig. 3b). The lack of absorbance strength here may be due to the very low amount of material analyzed.

Table 5. Main electronic transitions observed for the uranyl phosphate minerals from photoluminescence (PL) and diffuse reflectance experiments^a. H: hot band.

Mineral	PL transitions (nm)	Absorption transitions ^b (nm)
Ulrichite	482H, 498, 520, 544, 568, 594	401, 411, 422, 435, 448, 463
Uranocircite	489H 506, 527, 550, 576, 604	401, 413, 425, 437, 454, 469, 485, 502
Metatorbernite	487H 504, 526, 549, 576, 604	406, 418, 428, 442, 456, 470, 486, 502

PAPER

RSC Advances

Saleeite	482H 498, 518, 544, 570, 595	401, 411, 423, 437, 451, 465, 481, 497
Phosphuranylite	540 (poorly resolved)	422, 436, 448, 492

^aTransition energy can be obtained in cm^{-1} or eV by dividing 10^7 by the λ in nm or by dividing 1240 by the λ in nm, respectively. ^bDerived from diffuse reflectance spectra presented herein. See table S2 for energies in cm^{-1} and vibronic gaps.

Tables 5 and S2 compile the electronic transitions found in PL and reflectance spectra. The observed energies differ from one sample to another in the two techniques as well as the energy spacing in the ground state. On the whole, the fine and relatively intense structures in the spectra discussed here are in fair agreement with the absorptions or emissions of uranyl ions in solution given earlier.^[45] Accordingly, electronic spectroscopy (absorption or radiative emission) constitutes another efficient tool to ultimately trace the nature of uranyl phosphate materials.

4 Conclusions

In summary, direct spectroscopic detection of natural uranyl phosphate hydrates has been carried out by using Raman, infrared, diffuse reflectance and photoluminescence spectroscopy. The vibrational features of the uranyl cation and phosphate anion identified by these techniques are specific for each studied mineral. The variations of frequencies and wavelengths from one mineral to another can be used as markers in mineral identification relevant for environmental sustainability. It is demonstrated here for the first time that the vibronic structure of uranyl phosphorescence and diffuse reflectance in U^{VI} -containing minerals provides also a reliable electronic fingerprint for identifying these compounds. Additionally, the water bands of the infrared spectra can help in the tagging of the minerals. These experimental results supported by theoretical calculations offer innovation in affordable characterization probes permitting to look at raw minerals issued from geologic samples or present in groundwater aquifers without further material processing and in a short time-frame. In particular, portable Raman spectrometers can be used easily in situ in soils or waters to check efficiency of uranium uptake by phosphate minerals. Phosphate remediation to diminish hazards related to uranium in groundwater aquifers and to depleted uranium from ammunition weaponry in war zones^[46] could be efficiently monitored this way.

Acknowledgements

One of the authors (DLP) was supported by the U. S. Department of Energy under Contract No. DE-ACO3-76SF00098. EF thanks Dr Karine Costuas from the University of Rennes for useful advices. The referees are acknowledged for valuable comments.

References

- G. Bernhard, G. Geipel, V. Brendler, H. Nitsche, *J. Alloys Compd.*, **1998**, 271-273, 201-205.
- S. A. Shaw, M. J. Hendry, J. Essilfie-Dughan, T. Kotzer, D. Wallschlager, *Appl. Geochem.*, **2011**, 26, 2044-2056.

- R. J. Bowell, J. Grogan, M. Hutton-Ashkenny, C. Brough, K. Penman, D. J. Sapsford, *Miner. Eng.*, **2011**, 24, 1305-1313.
- Y. Ohashi, M. Nomura, Y. Tsunashima, S. Ando, N. Sugitsue, Y. Ikeda, Y. Tanaka, *J. Nucl. Sci. Technol.*, **2014**, 51, 251-265.
- D. Gryaznov, E. Heifets, E. Kotomin, *Phys. Chem. Chem. Phys.*, **2012**, 14, 4482-4490.
- M. Dittmar, *Energy*, **2012**, 37, 35-40.
- A. C. Perkins, *Eur. J. Nucl. Med. Mol. Imaging*, **2013**, 40, 979-981.
- S. E. Hines, P. Gucer, S. Kligerman, R. Breyer, J. Centeno, J. Gaitens, M. Oliver, S. Engelhardt, K. Squibb, M. McDiarmid, *J. Occup. Environ. Med.*, **2013**, 55, 937-944.
- M. Kulich, V. Rericha, R. Renricha, D. L. Shore, D. P. Sandler, *Environ. Res.* **2011**, 111, 400-405.
- R. A. Crane, M. Dickinson, I. C. Popescu, T. B. Scott, *Water Res.*, **2011**, 45, 2931-2942.
- A. Sakaguchi, A. Kadokura, P. Steier, Y. Takahashi, K. Shizuma, M. Hoshi, T. Nakakuki, M. Yamamoto, *Earth. Planet. Sci. Lett.*, **2012**, 333-334, 165-170.
- K. Chandrasekaran, D. Karunasagar, J. Arunachalam, *Anal. Methods* **2011**, 3, 2140-2147.
- D. M. Wellman, K. M. Gunderson, J. P. Icenhower, S.W. Forrester, *Geochem. Geophys. Geosyst.*, **2007**, 8, 1-16; D. Gorman-Lewis, T. Shvareva, K.-A. Kubatko, P. C. Burns, D. M. Wellman, B. McNamara, J. E. S. Szymanowski, A. Navrotsky, J. B. Fein, *Environ. Sci. Technol.*, **2009**, 43, 7416-7422.
- A. J. Locock, P. C. Burns, *Canad. Mineral.*, **2003**, 41, 489-502.
- F. Demartin, V. Diella, S. Donzelli, C. M. Gramaccioli, T. Pilati, *Acta Cryst.*, **1991**, B47, 439-446.
- S. A. Miller, J. C. Taylor, *Z. Kristallogr.*, **1986**, 177, 247-253.
- U. Kolitsch, G. Giester, *Mineral. Mag.*, **2001**, 65, 717-724.
- A. V. Barinova, R. K. Rastsvetaeva, G. A. Sidorenko, N. V. Chukanov, D. Y. Pushcharovskii, M. Pasero, S. Merlini, *Dokl. Chem.* **2003**, 389, 58-61; A. J. Locock, P. C. Burns, T. M. Flynn, *Canad. Mineral.*, **2005**, 43, 721-733.
- G. S. Groenewold, A. K. Gianotto, and M. E. Mclwain, M. J. Van Stipdonk, M. Kullman, D. T. Moore, N. Polfer, J. Oomens, I. Infante, L. Visscher, B. Siboulet, W. A. de Jong, *J. Phys. Chem. A*, **2008**, 112, 508-521
- H-Z. Yu, C. Li, B-H. Chen, C-T. Yang, D. Wang, Y. Fu, S. Hu, Z. Dang, *RSC Adv.*, **2014**, 4, 50261-50270.
- <http://rruff.info/>
- J. Cejka Jr, A. Muck, J. Cejka, *Phys. Chem. Miner.*, **1984**, 11, 172-177.
- R. L. Frost, *Spectrochim. Acta A*, **2004**, 60, 1469-1480.
- R. L. Frost, J. Cejka, M. Weier, G. A. Ayoko, *Spectrochim. Acta A*, **2007**, 66, 979-984.
- R. L. Frost, J. Cejka, G. A. Ayoko, M. Weier, *J. Raman Spectrosc.*, **2006**, 37, 1362-1367.
- R. L. Frost, J. Cejka, G. A. Ayoko, *J. Raman Spectrosc.*, **2008**, 9, 495-502.
- R. P. J. Driscoll, D. Wolverson, J. M. Mitchels, J. M. Skelton, S. C. Parker, M. Molinari, I. Khan, D. Geeson, G. C. Allen, *RSC Adv.*, **2014**, 4, 59137-59149.
- N. Sanchez-Pastor, A. J. Pinto, J. M. Astilleros, L. Fernandez-Diaz, M. A. Gonçalves, *Spectrochim. Acta A.*, **2013**, 113, 196-202.
- E. Faulques, R. Russo, D.L. Perry, *Spectrochim. Acta A*, **1993**, 49, 975-983.
- E. Faulques, R. Russo, D.L. Perry, *Spectrochim. Acta A*, **1994**, 50, 757-763.

- 31 M. Pham-Thi, P. Colomban, *J. Less-Common. Met.*, **1985**, *108*, 189-216.
- 32 K. M. Ok, J. Baek, P. S. Halasyamani, D. O'Hare, *Inorg. Chem.*, **2006**, *45*, 10207-10214.
- 33 R.M. Badger, *J. Chem. Phys.*, **1935**, *3*, 710-714
- 34 L. H. Jones, *Spectrochim. Acta*, **1959**, *15*, 409.
- 35 J. R. Bartlett, J.P. Cooney, *J. Mol. Struct.*, **1989**, *193*, 295.
- 36 W. W. Rudolph, G. Irmer, *Appl. Spectr.*, **2007**, *61*, 1312-1327.
- 37 V. Pomogaev, S. Prakash Tiwari, N. Rai, G. S. Goff, W. Runde, W. F. Schneider, E. J. Maginn, *Phys. Chem. Chem. Phys.*, **2013**, *15*, 15954-15963; N. B. Colthup, L. H. Daly, S. E. Wiberley, *Introduction to Infrared and Raman spectroscopy*, Academic Press Inc., San Diego, **1990**.
- 38 J. M. Aguirre, A. Gutiérrez, O. Giraldo, *J. Braz. Chem. Soc.*, **2011**, *22*, 546-551.
- 39 A. Paz, D. Guadarrama, M. López, J. E. González, N. Brizuela, J. Aragón, *Quim. Nova*, **2012**, *35*, 1724-1727.
- 40 E. Fritsch, L. Mihut, M. Baibarac, I. Baltog, M. Ostrooumov, S. Lefrant, J. Wéry, *J. Appl. Phys.*, **2001**, *90*, 4777-4782.
- 41 E. Fritsch, T. Spano-Franco, P. Megaw, *The Journal of Gemmology*, **2014**, *34*, 294-296.
- 42 Z. Wang, J. M. Zachara, P. L. Gassman, C. Liu, O. Qafoku, W. Yantasee, J. G. Catalano, *Geochim. Cosmochim. Acta*, **2005**, *69*, 1391-1403.
- 43 M. Del Nero, C. Galindo, R. Barillon, B. Madé, *Environ. Sci. Technol.*, **2011**, *45*, 3982-3988.
- 44 C. K. Jørgensen, R. Reisfeld, *J. Electrochem. Soc.*, **1983**, 681-684.
- 45 G. Meinrath, *J. Radioanalyt. Nucl. Chem.*, **1997**, *224*, 119-126.
- 46 N. Baumann, T. Arnold, H. Foersterdorf, D. Read, *Environ. Sci. Technol.*, **2008**, *42*, 8266-8269.

Entry for the Table of Contents

Uranyl phosphate minerals are studied by optical and vibrational spectroscopy which provide robust markers to discriminate among environmentally hazardous uranium phases

